Bioinspired Superhydrophobic Surface Constructed from Hydrophilic Building Blocks: A Case Study of Core–Shell Polypyrrole-Coated Copper Nanoneedles

Yang Liu [1,2,*], Ben Wang [3,4], Yuanfeng Wang [2], Jiareng Chen [1], Bin Cui [1], Pengfei Yin [1], Jianming Chen [2], Xinyu Zhang [5], Li Zhang [4] and John H. Xin [2,*]

[1] Department of Biomedical Engineering, Sun Yat-sen University, Guangzhou 510006, China; chenjr55@mail2.sysu.edu.cn (J.C.); cuib3@mail2.sysu.edu.cn (B.C.); yinpf3@mail2.sysu.edu.cn (P.Y.)

[2] Institute of Textiles and Clothing, Hong Kong Polytechnic University, Hung Hom, Kowloon, Hong Kong 999077, China; wangyuanfeng@cuhk.edu.cn (Y.W.); jamin-chen@hotmail.com (J.C.)

[3] College of Chemistry and Environmental Engineering, Shenzhen University, Shenzhen 518060, China; benwang@szu.edu.cn

[4] Department of Mechanical and Automation Engineering, Chinese University of Hong Kong, Hong Kong 999077, China; lizhang@mae.cuhk.edu.hk

[5] Department of Chemical Engineering, Auburn University, Auburn, AL 36849, USA; xzz0004@auburn.edu

* Correspondence: liuyang56@mail.sysu.edu.cn (Y.L.); tcxinjh@polyu.edu.hk (J.H.X.)

check for updates

Abstract: Hydrophilic polypyrrole-coated copper nanoneedles (PPy-CuNDs) were synthesized and utilized to construct a superhydrophobic surface on a polyethylene terephthalate fabric (PET) by using the spray-coating technique. The morphology of the as-synthesized PPy-CuNDs can be facilely tuned by changing the concentration of the reducing agent: hydrazine monohydrate. The CuNDs with well-defined nanocrystalline structures and nanoscale thick, rough PPy coating layers were formed simultaneously in one pot. The PPy-CuNDs self-assembled into an entangled, stacking nanocarpet on the surface of the PET fabric, and they eventually formed a reentrant surface texture similar to that of chrysanthemum leaves. The PPy-CuND-PET surface initially showed good superhydrophobic properties, but a fast transition from the superhydrophobic state to the highly adhesive state was observed. The underlying mechanism of this transition and its potential applications were proposed in the context.

Keywords: bioinspired; superhydrophobic surface; hydrophilic; polypyrrole; copper; nanoneedle

1. Introduction

Superhydrophobic surfaces widely exist on natural species, such as plants and insects, which are believed to originate from the combination of surface microstructures and wax [1,2]. For over 80 years, the development of superhydrophobic surfaces (SHS) has been focused on the creation of surface microstructures with low surface energy chemical coatings [3]. Various strategies, such as chemical etching, plasma treatment, photolithography, chemical vapor deposition, and electrostatic deposition are employed to create SHS with substantially high water contact angles, low hysteresis, oil repellency, and omniphobicity, e.g., the creation of a superhydrophobic lotus-leaf-like bioinspired surface [4], a superhydrophobic carbon nanotube forest [5], reentrantly textured silica micropillar arrays [6], an omniphobic slippery liquid infused porous surface [7], and a robust superhydrophobic metal surface [8]. However, these microstructured SHS may require additional low-surface-energy coatings, e.g., polytetrafluoroethylene, fluoroalkylsilanes, and perfluorinated fluids, to achieve and stabilize their superhydrophobic properties such as self-cleaning, droplet bouncing, and liquid repellency. Serious

health and environmental concerns are raised by the usage of the traditional fluorinated molecules, such as their toxicity to plants [9]. To address this issue, biocompatible fluorinated molecules, e.g., perfluoropolyether, were used to construct omniphobic surfaces and SHS via one-step 3D printing and stereolithography prototyping methods, respectively [10,11]. On the other hand, it is also feasible to construct SHS by using non-fluorinated hydrophilic building blocks. It has been reported that SHS can be constructed from the intrinsic hydrophilic materials with $\theta_Y < 90°$ by using different surface patterning strategies. For example, omniphobicity was realized on silica, tungsten, and parylene surfaces by creating microposts with doubly reentrant microstructures using photolithography [12]. The as-obtained microtextured surfaces can repel perfluorohexane with a surface tension as low as 10 mN m^{-1}. A superhydrophobic zinc oxide (ZnO) surface can also be obtained by growing lotus-leaf-like ZnO microspheres decorated with ZnO nanorods on a porous anodic alumina film using chemical vapor deposition [13]. Superhydrophobic copper (Cu) surfaces were fabricated by depositing Cu nanoparticles (NPs) on a silicon wafer with high surface coverage [14]. A superhydrophobic aluminum surface was prepared by thermally annealing a pre-etched aluminum sheet in air [15]. A superhydrophobic titania surface was constructed on the graphene-coated cotton fabrics [16]. It seems the Wenzel equation ($\cos\theta_A = r\cos\theta_Y$) does not fit to describe the SHS with $\theta_Y < 90°$, but we should consider the local geometries formed by the surface microstructures and their interactions with the liquid droplet rather than the roughness of the whole surface, when trying to describe SHS with air-pocket-forming textures.

Herein, we construct a new type of SHS by using hydrophilic copper (Cu) nanoneedles with nanoscale polypyrrole (PPy) coatings on their surface. The formation of the one-dimensional (1D) nanostructured Cu needles and the PPy coating on their surface was simultaneously achieved in one pot. The morphology of the PPy-coated Cu nanoneedles can be facilely tuned by changing the concentration of the reducing reagent. Even though both 1D Cu nanoneedles and the PPy coatings are intrinsically hydrophilic with $\theta_Y < 90°$, SHS can be formed by the random stacking of the PPy-coated Cu nanoneedles (PPy-CuNDs) on the surface of a woven polyethylene terephthalate (PET) fabric. The as-obtained PPy-CuND-PET surface showed high water repellency, i.e., a high water contact angle, bouncing of the impinging water droplets and low sliding angle, when the droplets were deposited on the SHS (Figure A1 in Appendix A). Afterwards, the water droplets that remained sitting on the SHS may start to pin, and they were difficult to roll off due to their adhesion to the SHS. However, the water droplets can maintain their pinned state on the SHS without further spreading. This phenomenon is quite different from the "lotus effect", as there is a transition on the droplets from the non-wetting Cassie state to the partial wetting Wenzel state. This transition can be possibly attributed to the hydrophilic interaction between the water droplet and PPy-CuNDs. The water droplet would slowly wet the uppermost surface layer of the stacking, entangled PPy-CuNDs, and eventually lead to the highly adhesive state.

2. Materials and Methods

2.1. Materials

Pyrrole (99%), copper chloride anhydrous (CuCl$_2$, 98%), and sodium hydroxide (NaOH, 96%) were purchased from Macklin Inc. Hydrazine monohydrate (N$_2$H$_4$·H$_2$O, >98%), and ethanol (C$_2$H$_5$OH, ≥99.5%) was purchased from Aladdin Co., Ltd. All chemicals were used without further purification.

2.2. Synthesis of PPy-CuNDs

First, 30 mL of 7M NaOH solution was placed in a 100-mL glass beaker; subsequently, 1 mL of 0.1 M CuCl$_2$ solution was added into the glass beaker under magnetic stirring. The CuCl$_2$ solution quickly dispersed in the NaOH solution, and the color of the mixture solution turned homogeneous light blue within tens of seconds. Subsequently, 0.5 mL of pyrrole was quickly injected into the mixture solution by using a 1-mL syringe. Due to the hydrophobicity of pyrrole, it may require at least 20

min high-speed magnetic stirring to homogeneously disperse it in the mixture solution. The color of the mixture solution would gradually turn dark brown during the dispersing process of pyrrole. Afterwards, hydrazine monohydrate was added into the mixture solution, and the temperature of the solution was slowly elevated to 60 °C on a heating plate. Then, the reaction was allowed to proceed at 60 °C for an hour. The concentration of the hydrazine monohydrate can be set to 9.60×10^{-3}, 1.60×10^{-2}, and 3.19×10^{-2} mol L^{-1}, respectively, in order to obtain PPy-CuNDs with different morphologies. As the reaction was complete, the as-obtained PPy-CuNDs were separated from the mixture by centrifuging (ST16R, Thermo Scientific) at 4000 rpm for 10 min. After centrifugation, the supernatant was decanted, and the PPy-CuNDs were re-dispersed in deionized water and ethanol for further purification. The centrifugation and re-disperse processes were repeated at least 3 times. Eventually, the as-obtained PPy-CuNDs were dried under ambient condition overnight before usage.

2.3. Fabrication of the Superhydrophobic PPy-CuND-PET Surface

The PPy-CuND-PET surface was prepared by using a simple spray-coating method. First, 5 mL of 1 mg mL^{-1} PPy-CuND isopropanol dispersion was prepared and loaded into a 7-mL spray gun equipped with a 3.0-L air pump. A plain-woven PET fabric was fixed on a hot plate (Cimarec, Thermo Scientific) by adhesive tape, and the temperature on the plate surface was set to 80 °C. Afterwards, the PPy-CuNDs were deposited onto the PET fabric through the spray gun. As the sprayed dispersion reached the fabric surface, the isopropanol quickly evaporated, leaving the PPy-CuNDs. The spray gun was operated at a short distance to the fabric surface, and the spraying process was conducted slowly to achieve a homogeneous coating.

2.4. Characterizations

A scanning electron microscope (SEM, JEOL JXA-8600) (JEOL Ltd., Tokyo, Japan) was used to characterize the morphology of the as-obtained PPy-CuNDs. High-resolution transmission electron microscope (HRTEM, JEOL JEM-2100F) (JEOL Ltd., Tokyo, Japan) was used to characterize the microstructure and lattice structure of the PPy-CuNDs. The average diameters and standard deviations were obtained by counting at least 50 individual PPy-CuNDs from the SEM and TEM images using ImageJ (delivered by National Institutes of Health, city, USA).

The water contact angle of the PPy-CuND-PET surface was measured by a contact angle measurement and contour analysis system (OCA-15 plus, Dataphysics) (DataPhysics Instruments GmbH, Filderstadt, Germany). A 2-μL water droplet was perpendicularly deposited onto the PPy-CuND-PET surface by an automated micro-syringe. The static water contact angle was measured by the OCA software using Young–Laplace fit. Five paralleled measurements were conducted at different points on the PPy-CuND-PET surface to obtain the average static water contact angle.

3. Results and Discussion

The PPy-CuNDs were synthesized by a one-pot method in aqueous alkaline solution based on our previous report [17]. $CuCl_2$ and pyrrole (Py) were added as the precursors, and hydrazine monohydrate was used as the reducing agent. It was speculated that the Py monomers would chelate to the Cu^{2+} cations, forming ligand–metal–charge–transfer (LMCT) complexes. The complexes would subsequently nucleate to induce the anisotropic growth of the CuNDs, and the polymerization of Py would be initiated simultaneously to form a nanocoating of PPy on the surface of the CuNDs [17]. The as-synthesized PPy-CuNDs showed a characteristic 1D nanostructure: the lengths of the PPy-CuNDs were much higher than their cross-sectional diameters, and the diameters on the two ends of the PPy-CuNDs were significantly different; a decreasing trend of the diameters can be observed between the bigger heads of the PPy-CuNDs and the smaller tails, similar to the "needles", as shown in Figure 1a,d. The average diameter of the PPy-CuNDs synthesized by the hydrazine concentration of 9.60×10^{-3} mol L^{-1} was calculated to be 132 ± 27 nm by counting the diameters in the middle. The average diameter of the bigger heads was calculated to be 229 ± 42 nm, and the average diameter of

the smaller tails was calculated to be 95 ± 16 nm. The morphology of the PPy-CuNDs can be easily tuned by using different hydrazine monohydrate concentrations. As the concentration of hydrazine monohydrate increased from 9.60×10^{-3} mol L^{-1} to 1.60×10^{-2} mol L^{-1}, both the average diameter and the lengths of the PPy-CuNDs increased (Figure 1b,e). At this time, the average diameter of the as-synthesized PPy-CuNDs was calculated to be 392 ± 74 nm. Large particulates with the size of a few hundreds of nanometers and tiny PPy-CuNDs with the diameters around 70–130 nm were found to deposit on the surface of the as-obtained PPy-CuNDs (Figure S1). It was speculated that the PPy-CuNDs would grow through the atomic addition of the diffusing Py-Cu^{2+} complexes. At higher hydrazine monohydrate concentrations, the addition rate would be faster, resulting in uneven growth rates at different nucleation sites and induces the formation of the particulates. On the other hand, the large PPy-CuNDs may also grow by consuming the small PPy-CuNDs through the Ostwald ripening process. By further increasing the hydrazine monohydrate concentration to 3.19×10^{-2} mol L^{-1}, the tiny PPy-CuNDs were disappeared as a result of the Ostwald ripening, and the average diameter of the as-synthesized PPy-CuNDs significantly increased to 1029 ± 249 nm (Figure 1c,f).
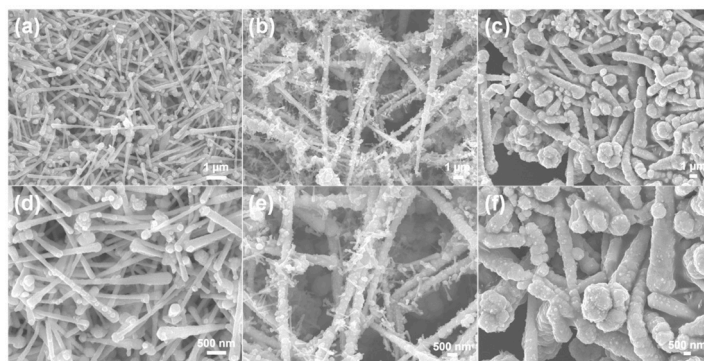

Figure 1. (**a**–**c**) SEM and (**d**–**f**) magnified SEM images of the polypyrrole-coated copper nanoneedles (PPy-CuNDs) synthesized in different hydrazine monohydrate concentrations: (**a**,**d**) 9.60×10^{-3} mol L^{-1}, (**b**,**e**) 1.60×10^{-2} mol L^{-1}, (**c**,**f**) 3.19×10^{-2} mol L^{-1}.

The thick heads and thin tails of the PPy-CuNDs showed a remarkable different contrast in the TEM image (Figure 2a). Due to the lower transmission of electrons, the thick heads were observed to be darker; whilst the thin tails were observed to be lighter as a result of the higher transmission of electrons. A different contrast can also be observed between the metallic cores of the CuNDs and the PPy nanocoating, as the PPy nanocoating was observed to be lighter in the TEM image. The magnified view of a single PPy-CuND was shown in Figure 2b. An ultra-thin layer of PPy can be observed on the surface of the CuND, covering most of the surface area of the CuND. Due to the different electron transmission property between the CuND core and the PPy coating, the lattice structure of the CuNDs can still be observed with the existence of a PPy coating layer on the surface. This phenomenon was more discernible at higher TEM magnifications (Figure S2). The morphology of the PPy coating layer was not smooth, and it was composed of aperiodic serrated microtextures, as shown in Figure 2c. The average height of the serrated structures was measured to be 16 ± 4 nm, according to the TEM images. The serrated microtextures formed by the PPy coating were presented as divided convex protuberances, and concave voids were formed between the two protuberances. The combination of concave and convex textures of the PPy coating resembles the previously reported "re-entrant" surface textures, and they have shown high non-wetting properties toward both water and low-molecular-weight hydrocarbons, as a result of the formation of a metastable solid–liquid–air three-phase contact line within the concave curvature [6,18]. The TEM image of a single PPy-CuND was shown in Figure 2d. The PPy-CuNDs showed thick heads, thin tails, and relatively straight side surfaces, resembling the shape of a "needle". The thickness of the PPy coating layer from head to tail was observed to decrease along the axial direction of the CuNDs. The lattice spacing of the CuND core was measured to be

0.21 nm according to the HRTEM image shown in Figure 2e. This value is coincident with the {111} reflection of the face-centered cubic (fcc) Cu. The selected area electron diffraction (SAED) pattern of the CuND core indicated that it was a piece of single crystalline grown in the {110} direction (Figure S3). The HRTEM image of a PPy protuberance was shown in Figure 2f. No crystalline structure can be observed in the imaging area, indicating that the PPy coating was amorphous.
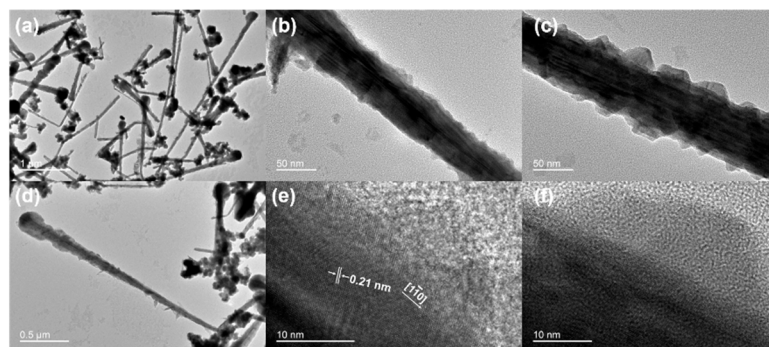

Figure 2. (**a**–**d**) TEM and (**e**,**f**) HRTEM images of the PPy-CuNDs synthesized at the hydrazine monohydrate concentration of 9.60×10^{-3} mol L^{-1}. The morphologies of single PPy-CuNDs were shown in (**b**–**d**). The lattice structure of the CuND core and the microstructure of the PPy nanocoating in (**d**) were shown in (**e**,**f**), respectively.

The re-entrant surface structures, i.e., nanofiber mats and microhoodoo arrays, can be used to construct non-wetting, super-repellent surfaces to both water and oils with and without the low-surface-energy fluoroalkyl silane coatings [6,12]. The re-entrant surface structures are typically composed of either randomly distributed or ordered microarrays of convex microstructures. The convex microstructures are acting as the solid fraction to support the liquid droplets, while the concave voids between the convex structures are acting as the air fraction to support the droplets. By controlling the spacing and geometric parameters (e.g., radius, height, width) of the convex structures, the solid fraction of the liquid–air–solid three-phase contact line can be minimized, resulting in a robust metastable superhydrophobic state with contact angles larger than 150°. To speak further, the sizes of the surface textures formed by both nanofibers and microhoodoos are in the micrometer range. It makes the unsilanized microhoodoos sufficient to support micrometer-size water droplets sitting on their surfaces, with contact angles as high as 143°; on the other hand, the nanofiber mat composed of poly(methyl methacrylate) can also reach a water contact angle around 130°, without the addition of fluorinated components [18]. However, by adding vertical overhangs on the microhoodoos and minimizing the surface solid fraction, a doubly reentrant structured surface was created, which was able to repel liquids with surface tensions as low as 10 mN m^{-1} [12].

By using the spray-coating technique, we deposited the PPy-CuNDs on the surface of a plain-weave PET fabric. Compared with the bare and smooth surface of the uncoated PET fabrics (Figure S4), a dense carpet of PPy-CuND was formed on the PET fabric's surface after spray-coating (Figure S5). The magnified SEM images of the PPy-CuND carpet at different surface locations (Figure 3a–c) indicated that the PPy-CuNDs were randomly stacking without specific orientations. The original surface structures of the fabric, i.e., the grains, warp, and weft yarns, can still be identified after the spray-coating process, indicating that the as-formed carpet of PPy-CuND was thin. The magnified SEM images at different coating locations are shown in Figure 3d–f. It can be observed that the 1D PPy-CuNDs were randomly stacked and interwoven, forming a porous nanocarpet on the PET fabric's surface. Due to the randomly stacking nature of the 1D PPy-CuNDs, the nanopores formed by the vacancies among the stacking PPy-CuNDs have a wide range of size distribution from a few nanometers to several hundreds of nanometers. These pores constitute the concave geometry of the PPy-CuND-coated PET surface (PPy-CuND-PET). On the other hand, the short and rigid PPy-CuNDs were stacked onto each other by random angles; in this case, either end of the 1D PPy-CuNDs may

tilt outwards to form the surface layer of the coating, driven by the effects of spatial hindrance and gravity. The entangled, stacking PPy-CuNDs and their tilting ends may constitute the convex geometry of PPy-CuND-PET. Therefore, the nanocarpet formed by the stacking PPy-CuNDs along with the nanopores formed during the stacking process may constitute the reentrant structural features of the PPy-CuND-PET surface. In nature, several plant leaves obtain similar surface features to PPy-CuND-PET, such as lavender and chrysanthemum. The surfaces of lavender and chrysanthemum are composed of a layer of hairy trichomes, which branched and stacked to form a reentrant structure (Figure S6). The density of trichomes on the lavender leaf surface was relatively low, which made the whole surface texture relatively "open"; a "closed" surface texture was formed on the chrysanthemum leaf surface by the high-density trichomes, and it also showed a higher water repellency than the lavender leaves [19].
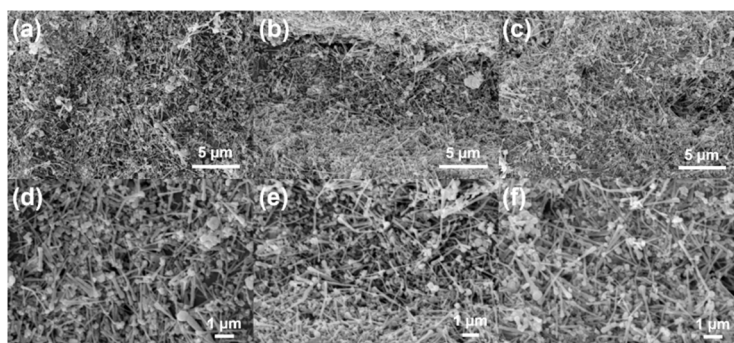
Figure 3. (**a**–**c**) SEM and (**d**–**f**) the corresponding magnified SEM images of the PPy-CuND coating on the PET fabric's surface, selected from different locations. The images of (**d**–**f**) are corresponded to (**a**–**c**), respectively.

A 3 × 3 matrix of 10 μL water droplets can be cast on the as-prepared PPy-CuND-PET surface and maintained their nearly spherical shape without observable spreading, as shown in Figure 4a. Thus, it indicated the strong hydrophobicity of the PPy-CuND-PET surface, which impeded the interpenetration of the water droplets through the microcapillaries within the PET substrate. A 2 μL water droplet was cast on the PPy-CuND-PET surface, and its image was captured by the charge-coupled device (CCD) camera, as shown in Figure 4b. The contact angle of the water droplet shown in Figure 4b was measured to be 156.6°, and the average contact angle of a 2-μL water droplet on the PPy-CuND-PET surface was measured to be 153.7° ± 2.0°, after measuring 5 different points on the PPy-CuND-PET surface. A 10-μL water droplet was cast on the PPy-CuND-PET surface from approximately 15 cm above the surface to evaluate its bouncing behavior on the PPy-CuND-PET surface, and the sequenced images showing the impinging and bouncing process of the droplet are presented in Figure 4c. From Figure 4c, we can observe that the 10-μL droplet barely bounced from the surface during the impinging process (from 0–140 ms). However, a smaller droplet was split from the 10-μL droplet during the contact (70 ms) and bounced off from the surface. After 170 ms (at 240 ms), the bounced droplet re-contacted the surface and re-bounced for a smaller height (270 ms), before the eventual immobilization on the surface (300 ms). The different bouncing behaviors observed between small and large droplets indicate that the superhydrophobic state on the PPy-CuND-PET surface is meta-stable. As the weight of impinging droplet increased, it would pin on the surface instead of bouncing off, indicating a high adhesion force between the droplet and the surface. On the other hand, a 10 μL water droplet freshly cast on the PPy-CuND-PET surface can be rolled off from the surface with a sliding angle smaller than 5°. However, it would pin on the surface if allowed to rest on the surface for 5 min. For example, the 3 × 3 matrix of 10-μL water droplets can be turned upside-down while the droplets remained adhered to the surface, as shown in Figure 4d. The observed phenomena indicated that the water droplets would tend to penetrate and wet the microcapillaries inside the PPy-CuND-PET surface, resulting in a fast transition from the superhydrophobic state to the highly adhesive state.
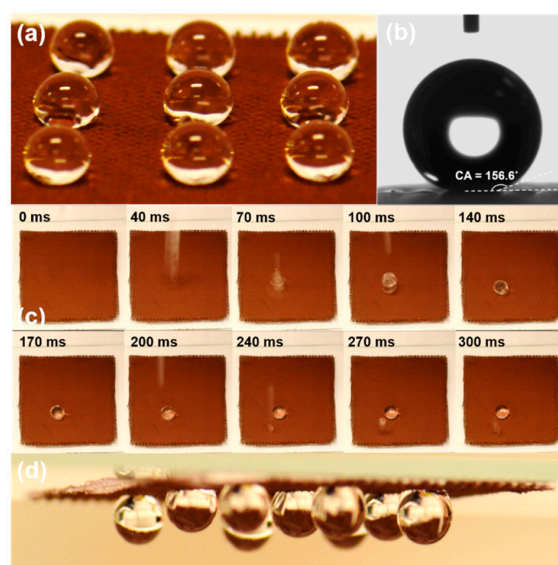
Figure 4. Photographs showing superhydrophobic properties of the PPy-CuND-PET surface. (**a**) A 3 × 3 matrix of 10-µL water droplets was cast on the surface and maintained their stability. (**b**) The contact angle of a 2-µL water droplet on the surface was measured to be 156.59°. (**c**) Sequenced images (from 0–300 ms) showed the bouncing process of a 10-µL impinging droplet. (**d**) The 3 × 3 matrix of 10-µL water droplets can be turned upside-down after 5 min static storage.

The fast transition from the superhydrophobic state to the highly adhesive state observed on the PPy-CuND-PET surface was speculated to be driven by the interaction between the water droplet and the local microstructure on the PPy-CuND-PET surface. To demonstrate the corresponding local microstructure, we use computer aided design (CAD) to simulate the 3D morphology of the PPy-CuND-PET surface, and the simulated PPy-CuND-PET surface with randomly stacking PPy-CuNDs is shown in Figure 5a. By rotating the 3D image of Figure 5a, we can obtain the cross-sectional view of the simulated PPy-CuND-PET surface in Figure 5b. In Figure 5b, we can observe that the free ends of the tilted PPy-CuNDs constitute the outermost layer of the PPy-CuND-PET surface. Now, consider a water droplet with a radius of r resting on the free ends of the PPy-CuNDs. As the water droplet interacts with the PPy-CuND-PET surface, its weight is supported by the free ends of a PPy-CuND and the cavities among them; the situation is demonstrated in Figure 5c in a simplified manner. The single unit of the droplet-supporting surface structure can be composed of two adjacent PPy-CuNDs and the cavity formed between them, as shown in Figure 5c. In the ideal circumstance, by treating the PET substrate as a flat plate and setting the two adjacent PPy-CuNDs aligned perpendicularly to the PET substrate, the local surface profile of the droplet in contact with the supporting unit would tend to form a meniscus inside the cavity of the two adjacent PPy-CuNDs by the combining force of surface tension and pressure, as shown in Figure 5c and Figure S7. As the weight of the droplet increases, the force also increases and further stretches the liquid to enter the cavity, resulting in the downward shifting of the three-phase contact point. At this stage, the local contact angle θ^* between the liquid and the PPy-CuND is apparently higher than 90°; and as the droplet weight increases, θ^* may also increase up to the superhydrophobic range (> 150°). During this stage, the droplets resting on the PPy-CuND-PET surface may show superhydrophobic properties, including a high contact angle, low sliding angle, and low hysteresis.

However, due to the hydrophilicity of the PPy-CuND surface, the contacted droplets would soon transform from the superhydrophobic state with a low sliding angle to the highly adhesive superhydrophobic state, while the existence of the hydrophilic, rough PPy nanocoating layer can even accelerate the transformation. By interpreting the interaction between the droplet and the local microstructure of the PPy-CuND-PET surface, the transition can be described by considering the shape

change of the water meniscus inside a single supporting unit. In Figure 5c, the single supporting unit consisting of two adjacent PPy-CuNDs and the cavity between them can be considered as a small capillary. As the surface of the PPy-CuNDs is hydrophilic (the contact angle of polypyrrole doped with chlorine ion is ca. 52.8° ± 3.2°) [20], the water inside the supporting unit would gradually wet the surface of the PPy-CuNDs and progress toward the bottom, driven by the capillary effect. During this process, the water meniscus inside the supporting unit may transform from the convex shape to the concave shape, resulting in a significant reduction in the local contact angle θ* from the hydrophobic range (>90°) to the hydrophilic range (<90°) and a significant increment of the adhesion force.
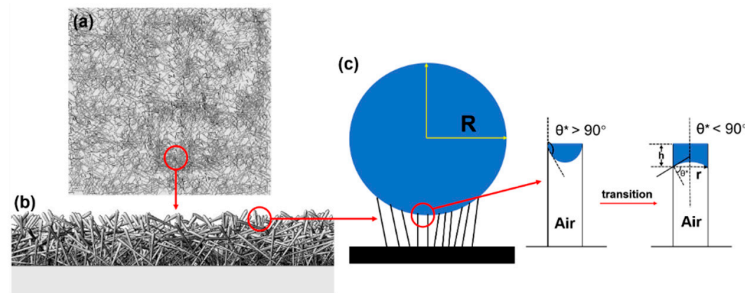
Figure 5. (**a**,**b**) 3D morphologies of the PPy-CuND-PET surface shown in (**a**) the top view and (**b**) the cross-sectional view. (**c**) Schematic illustration of a water droplet with radius r resting on the uppermost layer of the PPy-CuND-PET surface. The speculated transition of the water meniscus inside the capillary of a single supporting unit formed by two adjacent PPy-CuNDs and the cavity between them is also demonstrated.

The height (h) of the liquid inside the capillary can be calculated by considering the equilibrium of forces in the capillary. The downward force exerted by the surface tension and pressure on the liquid is balanced by the upward force exerted by the pressure of the entrapped air. For a capillary with a radius of r, there is:

$$P_0 \pi r^2 + 2\pi r \gamma \cos\theta^* + \rho g h \pi r^2 = (P_0 + \Delta P)\pi r^2 \tag{1}$$

where P_0 represents the atmospheric pressure, and γ and ρ represent the surface tension and density of water, respectively. g represents the acceleration gravity, and ΔP stands for the air pressure generated during balancing the downward force. By solving h using Equation (1), we can obtain:

$$h = \Delta P/\rho g - (2\gamma \cos\theta^*)/\rho g r. \tag{2}$$

By interpreting Equation (2), we can conclude that the value of *h* would decrease as the radius of capillary, *r*, is decreased. This trend is contradictory to the situation when a capillary is inserted into a water reservoir, where *h* is inverse proportional to *r*. This deduction indicates that for the SHS constructed from the hydrophilic 1D nanostructures, e.g., PPy-CuNDs, a shorter distance between the adjacent nanoneedles may help impede the transition from the superhydrophobic state to the highly adhesive state and improve the robustness of the as-obtained SHS.

4. Conclusions

In conclusion, we have successfully synthesized a core–shell nanostructure, CuND sheathed with a nanoscale-thin PPy coating layer, in a facile manner. By changing the concentration of the reducing agent, i.e., hydrazine monohydrate, the aspect ratio of the as-synthesized PPy-CuNDs can be easily tuned, while the thickness of the PPy coating layer was also observed to change along the CuNDs' axial direction. The PPy-CuNDs were subsequently utilized to fabricate a bioinspired superhydrophobic surface on a PET fabric surface, which mimicked the chrysanthemum leaf, by using the spray-coating method. The as-obtained PPy-CuND-PET surface initially showed excellent superhydrophobic

properties, including a high water contact angle, low sliding angle, and droplet bouncing. Then, a fast transition from the superhydrophobic state to a highly adhesive state may occur on the droplets. This transition is driven by both the water pressure and surface tension as well as the intrinsic hydrophilicity of the CuNDs and PPy. The rough morphology of the PPy nanocoating may accelerate the penetration and wetting of the water droplets inside the microcapillaries and formation of the highly adhesive state. The existence of the transition indicates that the superhydrophobic state observed on the PPy-CuND-PET surface is meta-stable. However, the capability of simultaneously maintaining a high water contact angle and high adhesion makes the PPy-CuND-PET surface quite attractive for the manipulation of microdroplets, which is important for biological reactions, microfluidic devices, traced analysis, and in situ detection [21–23]. These findings may help to develop a superhydrophobic surface based on reentrant structures that omits fluorinated coatings and design a superhydrophobic surface with tunable adhesion and particle retention.
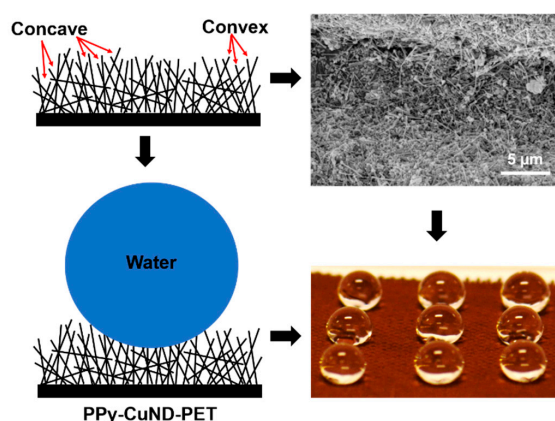
Appendix A

Figure A1. Hydrophilic Polypyrrole coated copper nanoneedles (PPy-CuND) with tunable morphologies were facilely synthesized in one-pot, and further used to construct superhydrophobic PPy-CuND-PET surface by spray-coating. The PPy-CuND-PET surface simultaneously showed high contact angles and high adhesion to water droplets, making it attractive for biological analysis and microfluidics.

References

1. Li, G.; Jiang, B.; Liu, H.; Ning, L.; Yi, D.; Wang, X.; Liu, Z. Superhydrophobic surface with lotus/petal effect and its improvement on fatigue resistance of heat-resistant steel. *Prog. Org. Coat.* **2019**, *137*, 105315. [CrossRef]
2. Nguyen, S.H.; Webb, H.K.; Mahon, P.J.; Crawford, R.J.; Ivanova, E.P. Natural insect and plant micro-/nanostructured surfaces: An excellent selection of valuable templates with superhydrophobic and self-cleaning properties. *Molecules* **2014**, *19*, 13614–13630. [CrossRef] [PubMed]
3. Teisala, H.; Tuominen, M.; Kuusipalo, J. Superhydrophobic coatings on cellulose-based materials: Fabrication, properties, and applications. *Adv. Mater. Interfaces* **2014**, *1*, 1300026. [CrossRef]
4. Ensikat, H.J.; Ditsche-Kuru, P.; Neinhuis, C.; Barthlott, W. Superhydrophobicity in perfection: The outstanding properties of the lotus leaf. *Beilstein J. Nanotechnol.* **2011**, *2*, 152–161. [CrossRef] [PubMed]
5. Lau, K.K.S.; Bico, J.; Teo, K.B.K.; Chhowalla, M.; Amaratunga, G.A.J.; Milne, W.I.; McKinley, G.H.; Gleason, K.K. Superhydrophobic carbon nanotube forests. *Nano Lett.* **2003**, *3*, 1701–1705. [CrossRef]
6. Tuteja, A.; Choi, W.; Mabry, J.M.; McKinley, G.H.; Cohen, R.E. Robust omniphobic surfaces. *Proc. Natl. Acad. Sci. USA* **2008**, *105*, 18200–18205. [CrossRef]
7. Wong, T.S.; Kang, S.H.; Tang, S.K.Y.; Smythe, E.J.; Hatton, B.D.; Grinthal, A.; Aizenberg, J. Bioinspired self-repairing slippery surfaces with pressure-stable omniphobicity. *Nature* **2011**, *477*, 443–447. [CrossRef]
8. Rodic, P.; Kapun, B.; Panjan, M.; Milosev, I. Easy and fast fabrication of self-cleaning and anti-icing perfluoroalkyl silane film on aluminium. *Coatings* **2020**, *10*, 234. [CrossRef]
9. Singh, G.; Kumari, B.; Sinam, G.; Kumar, N.; Mallick, S. Fluoride distribution and contamination in the water, soil and plants continuum and its remedial technologies, an Indian perspective—A review. *Environ. Pollut.* **2018**, *239*, 95–108. [CrossRef]
10. Credi, C.; Levi, M.; Turri, S.; Simeone, G. Stereolithography of perfluoropolyethers for the microfabrication of robust omniphobis surfaces. *Appl. Surf. Sci.* **2017**, *404*, 268–275. [CrossRef]
11. Credi, C.; Pintossi, D.; Bianchi, C.L.; Levi, M.; Griffini, G.; Turri, S. Combining stereolithography and replica molding: On the way to superhydrophobic polymeric devices for photovoltaics. *Mater. Design* **2017**, *133*, 143–153. [CrossRef]
12. Liu, T.; Kim, C.J. Turning a surface superrepellent even to completely wetting liquids. *Science* **2014**, *346*, 1096–1100. [CrossRef] [PubMed]
13. Li, Y.; Zheng, M.; Ma, L.; Zhong, M.; Shen, W. Fabrication of hierarchical ZnO architectures and their superhydrophobic surfaces with strong adhesive force. *Inorg. Chem.* **2008**, *47*, 3140–3143. [CrossRef] [PubMed]
14. Brink, G.H.; Foley, N.; Zwaan, D.; Kooi, B.J.; Palasantzas, G. Roughness controlled superhydrophobicity on single nanometer length scale with metal nanoparticles. *RSC Adv.* **2015**, *5*, 28696–28702. [CrossRef]
15. Cheng, Y.; Lu, S.; Xu, W. Controllable wettability of micro- and nano-dendritic structures formed on aluminum substrates. *New J. Chem.* **2015**, *39*, 6602. [CrossRef]
16. Liu, Y.; Wang, X.; Fei, B.; Hu, H.; Lai, C.; Xin, J.H. Bioinspired, stimuli-responsive, multifunctional superhydrophobic surface with directional wetting, adhesion, and transport of water. *Adv. Funct. Mater.* **2015**, *25*, 5047–5056. [CrossRef]
17. Liu, Y.; Liu, Z.; Lu, N.; Preiss, E.; Poyraz, S.; Kim, M.J.; Zhang, X. Facile synthesis of polypyrrole coated copper nanowires: A new concept to engineered core-shell structures. *Chem. Commun.* **2012**, *48*, 2621–2623. [CrossRef]
18. Tuteja, A.; Choi, W.; Ma, M.; Mabry, J.M.; Mazzella, S.A.; Rutledge, G.C.; McKinley, G.H.; Cohen, R.E. Designing superoleophobic surfaces. *Science* **2007**, *318*, 1618–1622. [CrossRef]
19. Challen, S.B. The retention of aqueous suspensions on leaf surfaces. *J. Pharm. Pharm.* **1962**, *14*, 707–714. [CrossRef]
20. Azioune, A.; Chehimi, M.M.; Miksa, B.; Basinska, T.; Slomkowski, S. Hydrophobic protein-polypyrrole interactions: The role of van der Waals and Lewis acid-base forces as determined by contact angle measurements. *Langmuir* **2002**, *18*, 1150–1156. [CrossRef]
21. Hong, X.; Gao, X.; Jiang, L. Application of superhydrophobic surface with high adhesive force in no lost transport of superparamagnetic microdroplet. *J. Am. Chem. Soc.* **2007**, *129*, 1478–1479. [CrossRef] [PubMed]

22. Yang, X.; Liu, X.; Lu, Y.; Zhou, S.; Gao, M.; Song, J.; Xu, W. Controlling the adhesion of superhydrophobic surfaces using electrolyte jet machining techniques. *Sci. Rep.* **2016**, *6*, 23985. [CrossRef] [PubMed]
23. Chen, C.; Zhang, L.; Sheng, M.; Guan, Y.; Dong, H.; Fu, S. Robust raspberry-like all-polymer particles for the construction of superhydrophobic surface with high water adhesive force. *J. Mater. Sci.* **2019**, *54*, 1898–1912. [CrossRef]